Received: 10 December 2024 | Revised: 26 February 2025 | Accepted: 23 April 2025 | Published online: 8 May 2025

RESEARCH ARTICLE

Medinformatics
2025, Vol. 2(3) 181–194
DOI: 10.47852/bonviewMEDIN52024995

BON VIEW PUBLISHING

In Silico Design of Novel *Artocarpus altilis*-Derived Compounds Targeting the c-Myc/Max Heterodimer

Tomilola Victor Akingbade[1,2,*], Ayobami Fidelix[3], Jatin Jangra[4], Olutola Adeyemo[5], Damilola Adeniyi[6] and Dolapo Damilola Akinlose[7]

[1]*Department of Biochemistry, University of Ibadan, Nigeria*

[2]*Computer-Aided Therapeutic Discovery and Design Platform, Federal University of Technology, Nigeria*

[3]*Department of Neurosurgery, University of Texas, USA*

[4]*Department of Pharmaceutical Engineering and Technology, Indian Institute of Technology, India*

[5]*Department of Obstetrics and Gynecology, Federal Teaching Hospital, Nigeria*

[6]*Department of Science Laboratory Technology, The Federal Polytechnic, Nigeria*

[7]*Department of Biochemistry, Ekiti State University, Nigeria*

Abstract: The transcription factor c-Myc plays a pivotal role in regulating cell proliferation, growth, apoptosis, metabolism, and differentiation; however, its overexpression is strongly linked to cancer. Due to its intrinsically disordered structure, c-Myc has been inherently challenging to target therapeutically. To exert its oncogenic effects, c-Myc must form a heterodimer with its binding partner Max, enabling DNA binding and transcriptional activation of target genes. Despite decades of research, developing effective c-Myc inhibitors remains challenging due to issues such as low potency and poor pharmacokinetics. Here, we investigate natural compounds derived from *Artocarpus altilis* as potential c-Myc inhibitors using computational methods. From screening 81 bioactive compounds, four candidates demonstrated stronger binding affinities to c-Myc than the reference drug Alisertib: Ellagic acid, Artonin M, Cycloaltilisin 7, and Broussoflavonol F. Molecular dynamics simulations showed Broussoflavonol F had exceptional stability and the most favorable MM-PBSA binding energy. Pharmacokinetic analysis suggested promising drug properties, though some toxicity risks were noted. These findings highlight *Artocarpus altilis*-derived compounds, particularly Broussoflavonol F, as promising c-Myc inhibitors. This study provides a foundation for experimental validation and optimization, offering new therapeutic potential against c-Myc-driven cancers.

Keywords: c-MYC inhibition, *Artocarpus altilis*, molecular docking, molecular dynamics, natural compounds, cancer therapeutics

1. Background Study

The c-myc (MYC) proto-oncogene, a key transcription factor characterized by its basic helix-loop-helix leucine zipper (bHLH-LZ) structure, significantly influences cellular dynamics, such as proliferation, growth arrest, apoptosis, and the suppression of cellular differentiation [1]. Strikingly, MYC overexpression is estimated to occur in a staggering up to 70% of various human cancer types [2]. Moreover, numerous studies have unequivocally demonstrated that MYC drives cancer progression by enabling key characteristics such as avoiding programmed cell death, sustaining proliferative signals, inducing genomic instability, escaping immune surveillance, and reprogramming metabolism [3, 4]. Despite its central role in cancer progression, direct targeting of MYC remains challenging due to its unstructured nature and complex regulatory mechanisms.

MYC forms a dimer with its small partner protein MAX, another bHLH-LZ protein, and notably influences the expression of approximately 15% of the human genome [5]. The MYC-MAX heterodimer binds particularly to palindromic E-box sequences in promoter regions, facilitating the recruitment of chromatin remodeling complexes [6] and transcription initiation machinery [7], thereby regulating the transcription of target genes. Additionally, the human MYC gene is situated on chromosome 8 at locus 8q24.21 and is intricately controlled at both transcriptional and translational levels [8]. MYC deregulation primarily occurs through gene alterations and the activation of upstream signaling pathways, such as NOTCH, WNT, and EGFR [3]. Furthermore, MYC is a very unstable protein with a brief half-life [5], and its stability is influenced by post-translational changes [8].

MYC stability is tightly regulated through phosphorylation and cis-trans isomerization, which direct its degradation via the ubiquitin–proteasome system. Two conserved sites within MYC's

***Corresponding author:** Tomilola Victor Akingbade, Department of Biochemistry, University of Ibadan and Computer-Aided Therapeutic Discovery and Design Platform, Federal University of Technology, Nigeria. Emails: takingbade7459@stu.ui.edu.ng; victomilola@gmail.com

transactivation domain, Serine 62 (Ser-62) and Threonine 58 (Thr-58) [9], are pivotal in this process. Phosphorylation at Ser-62 by kinases such as ERK1 and CDK2 stabilizes MYC, while subsequent phosphorylation at Thr-58 by GSK-3β or BRD4 marks it for breakdown. These modifications are governed by signaling pathways like Ras/Raf/ERK1 and PI3K/Akt, which modulate GSK-3β activity. The isomerase Pin1 further regulates MYC by altering the conformation of proline 63, enhancing its transcriptional activity before facilitating degradation. The interplay between Ser-62 stabilization and Thr-58 degradation is crucial for MYC function during cell proliferation, and disruptions in this balance are closely linked to cancers such as Burkitt lymphoma [10].

Mutations affecting MYC or its SCFFbw7 ubiquitin ligase binding site often lead to MYC stabilization, driving cancer progression in conditions like lymphomas and leukemias. Recent research also highlights the discovery of a second phospho-degron (Thr-244/Thr-248) that may synergize with the Thr-58/Ser-62 degron to enhance SCFFbw7 binding. This suggests that MYC degradation mechanisms are more complex than previously understood, requiring further study to refine current models. Additionally, BRD4 plays an essential role in Thr-58 phosphorylation, making it a critical regulator of MYC stability and a promising therapeutic target in MYC-driven cancers.

Despite promising candidates under investigation in preclinical and clinical studies [4], no MYC inhibitor has been approved to date. The main challenges with identified compounds include low potency, poor selectivity, and suboptimal pharmacokinetics, which limit their ability to reach sufficient concentrations to disrupt MYC-MAX dimerization [11]. Previous in silico studies have explored various small molecules as potential c-MYC inhibitors. For instance, L755507 has been identified as a novel inhibitor that disrupts c-MYC/MAX heterodimerization [12], while other studies have focused on natural compounds and their binding affinities to c-MYC. Our work builds on these findings by systematically screening *Artocarpus altilis*-derived compounds, which have not been extensively explored for c-MYC inhibition.

Natural products serve as a rich and diverse reservoir for discovering novel therapeutic agents [13]. Breadfruit (*Artocarpus altilis*) belongs to the Moraceae family and gets its common name from its bread-like appearance. The plant contains various phenolic substances including flavonoids, stilbenoids, and a lectin called jacalin. Different parts of the plant – from its fruit and leaves to its bark and stem – contain compounds that show promise for medical applications. Research has demonstrated that these bioactive substances have multiple therapeutic effects, such as fighting bacteria, tuberculosis, viruses, and fungi. They may also help with arthritis, prevent blood clots, inhibit tyrosinase, and show toxic effects on certain cells.

This study distinguishes itself by focusing on *Artocarpus altilis*-derived compounds, which have shown promising bioactivity but remain underexplored for c-MYC inhibition. Using a structure-based drug discovery approach, we targeted the drug-binding pocket within the MYC bHLH domain through molecular docking simulations. By integrating molecular docking, pharmacokinetic analysis, and molecular dynamics simulations, we provide a comprehensive evaluation of these compounds. The top-ranked compounds demonstrated strong binding affinity to the MYC bHLH domain, effectively disrupting its dimerization with the partner protein MAX. Our analysis identified novel candidates with superior binding affinities and stability compared to existing inhibitors, while providing crucial insights into their viability as potential drug candidates.

2. Experimental Procedures

The study employs a multi-step computational workflow to evaluate *Artocarpus altilis*-derived compounds as c-MYC inhibitors. Molecular docking identifies potential inhibitors based on binding affinity, pharmacokinetic analysis assesses drug-likeness and ADMET properties, and molecular dynamics simulations evaluate the stability and dynamic behavior of protein-ligand complexes. Finally, binding free energy calculations provide quantitative insights into the strength of interactions. This integrated approach ensures a comprehensive evaluation of the compounds, from initial screening to dynamic behavior in physiological conditions.

2.1. Ligand selection and preparation

A set of 81 bioactive compounds derived from *Artocarpus altilis* fruits, compiled from prior research [14, 15], were obtained from the PubChem database. Alisertib, an experimental aurora A kinase inhibitor under investigation for cancer treatment, served as a reference drug. All compound structures were converted from SDF to PDB format using Discovery Studio for subsequent ligand-protein docking assessments.

2.2. Protein-protein interaction

The three-dimensional structure of the unliganded c-MYC: MAX bHLHZip complex was obtained from the Research Collaboratory for Structural Bioinformatics (RCSB) Protein Data Bank (PDB ID: 6G6K) at a resolution of 1.35 Å. This crystal structure, derived from Homo sapiens and expressed in Escherichia coli, belongs to the functional category of apoptosis and contains no mutations [16]. The protein structure was refined using UCSF Chimera Software (v1.16). Protein-protein interaction examination was conducted using the Search Tool for the Retrieval of Interacting Genes/Proteins web server.

2.3. Molecular docking

Molecular docking studies can reveal the binding interactions between specific proteins and desired ligands [17]. Computational ligand-protein interaction assessment was carried out using AutoDock 4.2.6 following the preparation of the protein and ligand structures. The docking grid was established with dimensions of 24.1782 × 36.3133 × 37.1921, with the center coordinates at x: −61.3414, y: −59.8109, and z: −66.0998. The docking site was determined by amino acid residues within helix 1 (Arg913, Leu917, Ser920, Phe921, Leu924), the loop region (Gln927, Ile928), and helix 2 (Leu943, Ala946, Thr947, Tyr949, Ile950, Val953). As identified by Singh et al. [12], this site is situated in close proximity to the basic helix-loop-helix domain junction and aligns with the Myc–MAX heterodimer interface. The docking results were evaluated and prioritized based on their docking scores to determine the most favorable ligand-protein interactions.

2.4. Structural analysis and visualization

The strength of binding interactions for the top compounds was evaluated using PyMOL 3.10 and LigPlot software, with comparisons made to the reference drug, Alisertib. PyMol 3.10 was employed for visualizing the 3D protein-ligand interactions, while LigPlot V.2.2 was utilized for generating 2D representations [18, 19]. Table 1 shows the analysis involved a comprehensive examination of each ligand cluster, including the identification of amino acid residues interacting with the ligand, the determination

Table 1. Molecular interaction analysis of c-Myc with Ellagic acid, Artonin M, Cycloaltilisin 7, and Broussoflavonol F

Ligand-Protein complexes	Residues forming H-bonds	Residues involved in Hydrogen bond formation (Bond distances Å)	Hydrophobic interacting residues
c-Myc_Ellagic_acid	3	Glu935(3.04, 2.89), Ala937(2.95) Asp914(3.16)	Lys 936, Lys 918, Phe921, Leu917, Phe922, Lys939
c-Myc_ ArtoninM	0	None	Lys939, Arg914, Leu917, Lys918, Phe222, Ala937, Glu935, Lys936, Pro938, Val940
c-Myc_Cycloaltilisin 7	0	None	Pro938, Ala937, Ile942, Arg914, Lys918, Lys939, Lys936
c-Myc_ Broussoflavonol F	1	Lys918(3.27)	Pro938, Val940, Arg914, Leu917, Leu917, Phe922, Lys936, Ala937

of hydrogen bonds (H-bonds) formed, along with their respective distances (Å), and the detection of hydrophobic interactions.

2.5. Drug-likeness and ADMET prediction

The bioactive compounds from *Artocarpus altilis* fruits exhibiting the best binding affinity were further evaluated for their drug-likeness and bioavailability properties as shown in Table 2. To evaluate their suitability as drug candidates, these compounds were analyzed based on Lipinski's rule. The bioavailability score for each compound was determined using the SwissAdme online tool [20].

Furthermore, the ADMET properties (absorption, distribution, metabolism, elimination, and toxicity) of these compounds were assessed using the pkCSM web server [21]. This extensive evaluation aimed to pinpoint the most promising bioactive compounds derived from *Artocarpus altilis* fruits by analyzing their binding affinity, drug-likeness, bioavailability, and ADMET profiles, thus increasing their potential for further development as drug candidates.

2.6. Analysis of molecular dynamics simulation

Molecular dynamics simulations were employed to evaluate the stability of the top-ranked protein-ligand complexes and validate the docking results [17], using GROMACS 2020 software and the CHARMM-36M force field [22]. The initial structure for each MD simulation was based on the most stable docking conformation. Ligand topologies were generated through the CHARMM-GUI web interface [23]. The system was solvated using the TIP3P water model, with periodic boundary conditions applied. Neutralization of the system's charge was achieved via the Monte Carlo method by introducing Na+ and Cl− ions. Energy minimization was performed for 5000 steps using the steepest descent algorithm, while hydrogen bonds were constrained using the LINCS algorithm. The system was equilibrated for one nanosecond under NVT and NPT ensembles, employing the leap-frog integrator.

After equilibration, production runs of 100 nanoseconds were carried out under isothermal-isobaric conditions. Temperature (310.15 K) and pressure (1 bar) were controlled using the velocity-rescaling and Parrinello-Rahman methods. Post-simulation analysis focused on key parameters, including root mean square deviation (RMSD), root mean square fluctuation (RMSF), intermolecular hydrogen bonding, solvent-accessible surface area (SASA), and radius of gyration (Rg). These metrics were calculated using the built-in GROMACS tools: gmx_rms, gmx_rmsf, gmx_hbond, gmx_sasa, and gmx_gyrate. The data were visualized using the QtGrace plotting tool [24, 25].

This detailed MD simulation analysis offers valuable insights into the structural integrity and conformational behavior of the protein-ligand complexes, aiding in the drug design and optimization process.

2.7. Binding free energy analysis using MM-PBSA

Assessing the interaction strength between ligands and receptor proteins is essential in structure-based drug development. The Molecular Mechanics Poisson-Boltzmann Surface Area (MM-PBSA) method serves as a robust computational technique for estimating the binding free energies of non-covalent protein-ligand assemblies [26].

Table 2. Molecular docking and the drug-likeness results revealing the top 10 hit compounds and Alisertib

No.	Compounds	M/W g/mol	Docking scores	Lipinski violation	Bioavailability score
1	Alisertib*	518.92	−6.6	1	0.56
2	Ellagic acid	302.19	−7.2	0	0.55
3	Artonin M	502.56	−7.1	1	0.55
4	Cycloaltilisin 7	406.47	−7	0	0.55
5	Broussoflavonol F	422.47	−6.8	1	0.55
6	Cycloartenyl acetate	468.75	−6.7	1	0.55
7	Cycloheterophyllin	502.56	−6.7	1	0.55
8	Cyclocommunol	352.34	−6.6	0	0.55
9	Kazinol A	394.50	−6.5	0	0.55
10	Morin	302.24	−6.4	2	0.55
11	Cyclomorusin	418.44	−6.4	0	0.55

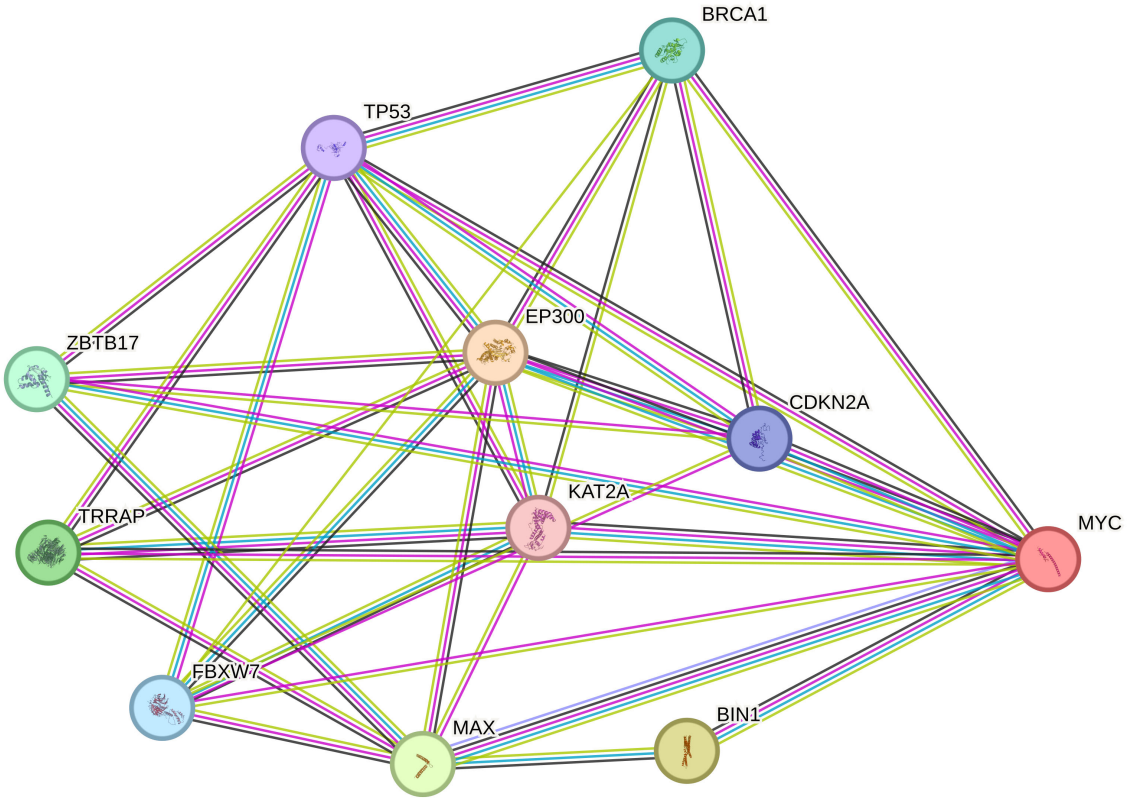

Figure 1. Protein-protein interaction profile of c-Myc

In our research, we utilized the gmx_MMPBSA program to determine the end-state free energies of chosen protein-ligand complexes. This Miniconda-based tool integrates GROMACS and Amber features using Python. The complexes were modeled for 100 ns in physiological conditions (310.15 K, 1 bar pressure) utilizing GROMACS 2020. The produced MD trajectory, topology, and index files were subsequently used to calculate the binding free energies [27]. This approach offers important perspectives on the energetics of protein-ligand interactions, aiding in the assessment and enhancement of possible drug candidates.

3. Results and Discussion

The docking results identify Ellagic acid, Artonin M, Cycloaltilisin 7, and Broussoflavonol F as potential c-MYC inhibitors, with binding affinities superior to the reference drug Alisertib. These findings address the study's objective of identifying novel inhibitors from *Artocarpus altilis*.

3.1. Protein-protein interaction (PPI)

Protein–protein interactions (PPIs) play a pivotal role in cellular function and regulation [28]. In healthy cells, PPIs stabilize multiprotein complexes, orchestrating nearly all cellular processes. Consequently, numerous PPIs have been identified as promising molecular targets for treating human diseases, including cancer. Despite the inherent challenges of targeting PPIs, significant progress has been made in drug discovery, with several small-molecule inhibitors advancing to clinical trials for cancer therapy [29, 30]. A deeper understanding of PPI networks and the structural mechanisms underlying these interactions has been instrumental in developing effective small molecules that disrupt these interfaces.

This study conducted a protein-protein interaction (PPI) analysis of the human c-MYC protein to identify its primary interacting partners. Key proteins predicted to interact with c-MYC include EP300 (Histone acetyltransferase p300), BIN1 (Myc box-dependent-interacting protein 1), MAX (Transcription regulator protein Max), TRRAP (Transformation/transcription domain-associated protein), ZBTB17 (Zinc finger and BTB domain-containing protein 17), BRCA1 (Breast cancer type 1 susceptibility protein), FBXW7 (F-box/WD repeat-containing protein 7), CDKN2A (Cyclin-dependent kinase inhibitor 2A), TP53 (Cellular tumor antigen p53), and KAT2A (Histone acetyltransferase KAT2A). These interactions, depicted in Figure 1, highlight the potential functional connections and regulatory roles of c-MYC and its binding partners, shedding light on the intricate signaling pathways and biological processes that this protein influences.

3.2. Molecular docking, drug-likeness and ADMET profiling

This study investigated the potential of several phytochemicals as c-MYC suppressors using molecular docking analysis. Among the compounds evaluated, Ellagic acid, Artonin M, Cycloaltilisin 7, and Broussoflavonol F exhibited superior docking scores compared to the reference drug, Alisertib, as shown in Table 2. Structural representations of these bioactive compounds are provided in Supplementary Figure 1. These results highlight their promising potential as c-MYC inhibitors. The findings align with the study's objective of identifying novel inhibitors derived from *Artocarpus altilis* and provide a strong rationale for further investigation into the selected compounds.

Figure 2 displays the binding conformations and interactions of these compounds with the target protein, emphasizing the

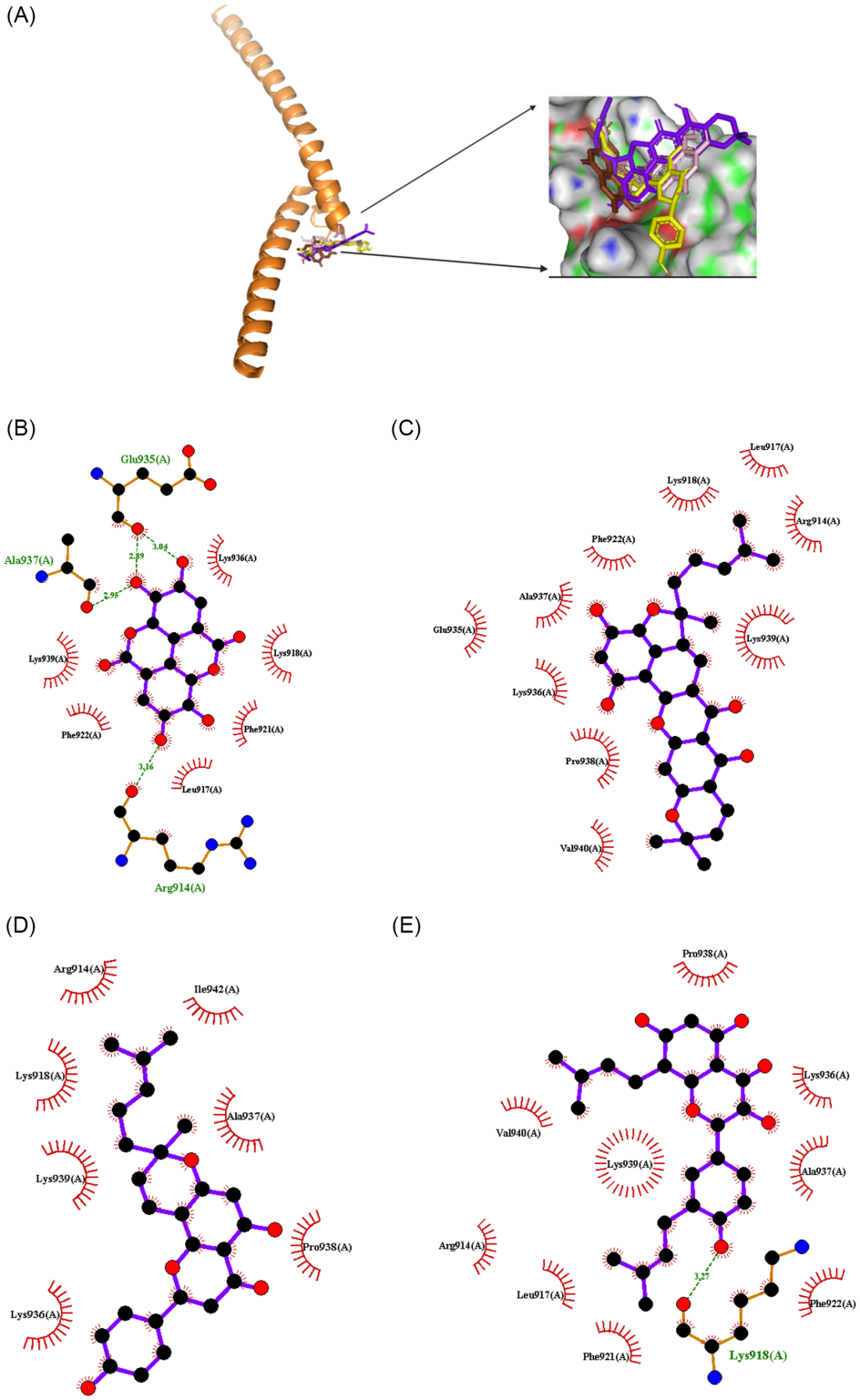

Figure 2. Molecular docking analysis of *Artocarpus altilis* phytocompounds and Alisertib with c-MYC. (A) Solvent-accessible surface view of the binding site, highlighting key amino acid residues. (B–E) 2D interaction diagrams for Ellagic acid, Artonin M, Cycloaltilisin 7, and Broussoflavonol F, showing hydrogen bonds and hydrophobic interactions.

involved amino acid residues, hydrogen bonds, bond distances, and hydrophobic interactions, with further details provided in Table 1.

The pkCSM web server was employed to comprehensively assess the drug-likeness and ADMET (Absorption, Distribution, Metabolism, Excretion, and Toxicity) properties of the top compounds [21]. Table 3 presents their pharmacokinetic profiles, detailing intestinal absorption, blood-brain barrier permeability, plasma protein binding, cytochrome P450 interactions, and toxicity risks.

All four compounds (Ellagic acid, Artonin M, Cycloaltilisin 7, and Broussoflavonol F) are predicted to have good human

Table 3. ADME prediction table

Compounds	Ellagic acid	Artonin M	Cycloaltilisin 7	Broussoflavonol F	Unit
ABSORPTION					
Water solubility	−3.181	−3.755	−4.38	−3.601	Numeric (log mol/L)
Caco-2 Permeability	0.335	0.419	1.137	0.108	Numeric (log Papp in 10−6 cm/s)
Intestinal absorption (human)	86.684	100	90.827	90.043	Numeric (% Absorbed)
Skin Permeability	−2.735	−2.735	−2.815	−2.735	Numeric (log Kp)
P-glycoprotein substrate	Yes	Yes	Yes	Yes	Categorical (Yes/No)
P-glycoprotein I inhibitor	No	Yes	Yes	Yes	Categorical (Yes/No)
P-glycoprotein II inhibitor	No	Yes	No	Yes	Categorical (Yes/No)
DISTRIBUTION					
VDss (human)	0.375	−0.328	0.651	−0.15	Numeric (log L/kg)
Fraction unbound (human)	0.083	0	0	0	Numeric (Fu)
BBB permeability	−1.272	−1.247	−0.242	−1.014	Numeric (log BB)
CNS permeability	−3.533	−2.844	−1.743	−1.965	Numeric (log PS)
METABOLISM					
CYP2D6 substrate	No	No	No	No	Categorical (Yes/No)
CYP3A4 substrate	No	Yes	Yes	Yes	Categorical (Yes/No)
CYP1A2 inhibitor	Yes	No	No	Yes	Categorical (Yes/No)
CYP2C19 inhibitor	No	Yes	Yes	Yes	Categorical (Yes/No)
CYP2C9 inhibitor	No	Yes	Yes	Yes	Categorical (Yes/No)
CYP2D6 inhibitor	No	No	No	No	Categorical (Yes/No)
CYP3A4 inhibitor	No	Yes	Yes	No	Categorical (Yes/No)
EXCRETION					
Total Clearance	0.537	−0.74	0.398	0.285	Numeric (log ml/min/kg)
Renal OCT2 substrate	No	No	No	No	Categorical (Yes/No)
TOXICITY					
AMES Toxicity	No	No	No	No	Categorical (Yes/No)
Max. tolerated dose (human)	0.476	0.04	−0.384	0.603	Numeric (log mg/kg/day)
hERG I inhibitor	No	No	No	No	Categorical (Yes/No)
hERG II inhibitor	No	Yes	No	Yes	Categorical (Yes/No)
Oral Rat Acute Toxicity (LD50)	2.399	2.293	2.604	2.562	Numeric (mol/kg)
Oral Rat Chronic Toxicity (LOAEL)	2.698	1.821	1.965	2.054	Numeric (log mg/kg_bw/day)
Hepatotoxicity	No	Yes	No	No	Categorical (Yes/No)
Skin Sensitization	No	No	No	No	Categorical (Yes/No)
T. Pyriformis toxicity	0.295	0.287	0.43	0.306	Numeric (log ug/L)
Minnow toxicity	2.11	−0.5	0.449	0.411	Numeric (log mM)

intestinal absorption (86.684%, 100%, 90.827%, and 90.043%, respectively), indicating positive oral bioavailability. However, Caco-2 permeability varies, with Cycloaltilisin 7 showing the highest permeability (1.137 log Papp) and Broussoflavonol F the lowest (0.108 log Papp). All compounds are predicted to be P-glycoprotein substrates, which has significant implications for their bioavailability and drug-drug interactions. Artonin M, Cycloaltilisin 7, and Broussoflavonol F are projected to be P-gp I inhibitors, while only Artonin M and Broussoflavonol F are expected to be P-gp II inhibitors. P-gp is an efflux transporter that limits the absorption of drugs in the intestine and promotes their excretion into bile and urine. While being a P-gp substrate can reduce oral bioavailability, it also helps in preventing the accumulation of toxic compounds in the body [31]. However, P-gp substrates are prone to drug-drug interactions when co-administered with P-gp inhibitors or inducers, which can alter their pharmacokinetics and efficacy. For example, Artonin M and Broussoflavonol F were predicted to be P-gp inhibitors, which could further complicate their use in combination therapies. This highlights the need for careful consideration of co-administered drugs during clinical development.

The volume of distribution (VDss) varies among the compounds, with Cycloaltilisin 7 showing the highest (0.651 log L/kg) and Artonin M the lowest (−0.328 log L/kg). All four compounds are predicted to have extensive plasma protein binding, with fraction unbound (Fu) values of 0.083 for Ellagic acid and 0 for the others, which may reduce their free concentrations and affect distribution and clearance. Regarding blood-brain barrier (BBB) permeability, Cycloaltilisin 7 shows the highest potential (−0.242 log BB), while the others have lower values, indicating limited BBB penetration. CNS permeability follows a similar trend, with Cycloaltilisin 7 having the highest value (−1.743 log PS) and Ellagic acid the lowest (−3.533 log PS).

None of the compounds are predicted to be CYP2D6 substrates, while Artonin M, Cycloaltilisin 7, and Broussoflavonol F are expected to be CYP3A4 substrates. Ellagic acid and Broussoflavonol F are projected to inhibit CYP1A2. Artonin M, Cycloaltilisin 7, and Broussoflavonol F are predicted to inhibit CYP2C19 and CYP2C9. Artonin M and Cycloaltilisin 7 are also expected to inhibit CYP3A4, the most abundant CYP450 enzyme responsible for metabolizing approximately 50% of clinically used drugs [32]. These interactions indicate potential drug-drug interactions. All compounds are predicted to exhibit favorable

clearance rates, with Ellagic acid showing the highest total clearance (0.537 log ml/min/kg) and Artonin M the lowest (−0.74 log ml/min/kg). The analysis suggests that none of the compounds will likely interact with the renal OCT2 transporter.

Furthermore, the results of the Ames test indicate that none of the compounds are expected to induce mutations. The maximum tolerated dose in humans varies, with Broussoflavonol F having the highest (0.603 log mg/kg/day) and Cycloaltilisin 7 the lowest (−0.384 log mg/kg/day). The compounds are not predicted to exhibit hERG I inhibition. However, both Artonin M and Broussoflavonol F are expected to inhibit hERG II, raising potential concerns regarding cardiotoxicity and the risk of QT interval prolongation, a serious side effect that can lead to fatal arrhythmias [33]. Oral rat acute toxicity (LD50) values range from 2.293 to 2.604 mol/kg, with Cycloaltilisin 7 showing the highest value. Chronic toxicity (LOAEL) values range from 1.821 to 2.698 log mg/kg_bw/day, with Ellagic acid having the highest value. Only Artonin M is predicted to be hepatotoxic. None of the compounds are expected to be skin sensitizers according to the pkCSM data. The compounds show varying toxicity levels to T. Pyriformis and Minnow, with Cycloaltilisin 7 having the highest toxicity for T. Pyriformis (0.43 log ug/L) and Ellagic acid for Minnow (2.11 log mM).

The ADMET predictions for the top compounds revealed promising drug-like properties, though some toxicity concerns were noted. This is consistent with previous studies on natural compounds, which often face challenges related to toxicity and bioavailability [29]. For example, while Ellagic acid and Artonin M showed favorable intestinal absorption, their potential hepatotoxicity and cardiotoxicity (hERG II inhibition) highlight the need for further optimization. These findings underscore the importance of balancing efficacy and safety in drug development, particularly for natural compounds.

3.3. Molecular dynamic simulations study

Molecular dynamics simulations (MDS) were conducted on the top-ranked docking conformations of four selected compounds (Ellagic Acid, Artonin M, Cycloaltilisin 7, and Broussoflavonol F). The MD simulations were used to validate the docking predictions by incorporating the dynamic nature of both the protein and ligand.

3.3.1. Root mean square deviation (RMSD)

Figure 3 presents the Root Mean Square Deviation (RMSD) profiles of selected ligands (Artonin M, Broussoflavonol F, Cycloaltilisin 7, and Ellagic acid) and the protein (cymc) compared to the reference drug, Alisertib, over a 100-nanosecond molecular dynamics simulation. Alisertib exhibits a gradual increase in RMSD, reaching ~9 nm, indicating significant conformational flexibility, while Artonin M, Broussoflavonol F, and Ellagic acid maintain stable RMSD values below 2 nm, suggesting consistent binding poses. Cycloaltilisin 7 shows notable fluctuations, with a sharp rise after 60 ns, peaking at ~9 nm, reflecting potential instability. The protein (cymc) remains stable, with RMSD fluctuations below 2 nm, confirming its structural integrity. These results highlight the robust binding of Artonin M, Broussoflavonol F, and Ellagic acid, contrasting with the instability of Cycloaltilisin 7 and the flexibility of Alisertib, providing critical insights into ligand-protein interactions and identifying promising candidates for further investigation.

3.3.2. Root mean square fluctuation (RMSF)

To further elucidate the structural dynamics, the backbone conformational variation and stability of the c-Myc_Alisertib, c-Myc_Broussolflavonol_F, c-Myc_Ellagic acid, c-Myc_Artonin M, and c-Myc_Cycloaltilisin 7 complexes were examined and visualized in Figure 4. The analysis revealed a common pattern across all complexes: significant fluctuations were observed within the first 20 amino acid residues, followed by a stabilization period spanning approximately 65 residues (from residue 20 to 85). Beyond the 85th residue, the complexes again exhibited fluctuations extending to the C-terminal end of the protein. This pattern suggests a central region of relative stability flanked by more dynamic N- and C-terminal regions in the c-Myc protein when complexed with these ligands. Figure 5 also shows the Ligand RMSF (Root Mean Square Fluctuation) plot of the selected ligands compared to the reference.

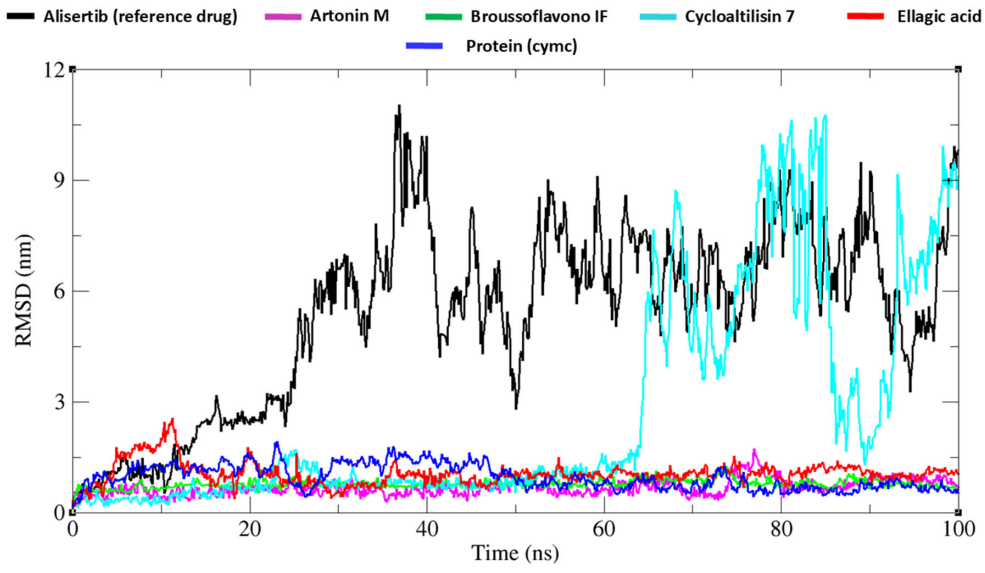

Figure 3. RMSD plot of the selected ligands in comparison with the reference (Alisertib)

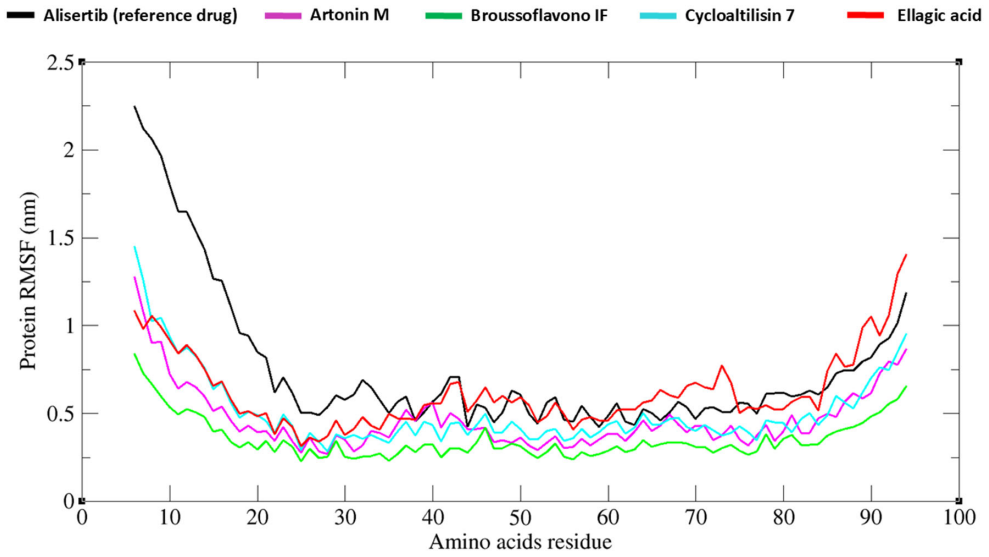

Figure 4. Protein RMSF plot for the selected ligands compared to the reference (Alisertib)

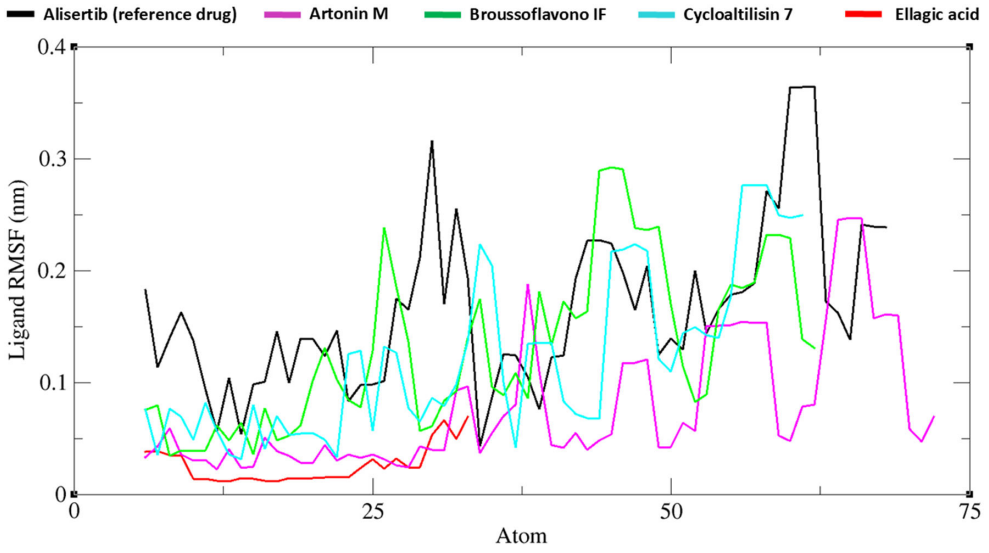

Figure 5. Ligand RMSF plot of the promising ligands compared to reference (Alisertib)

3.3.3. Hydrogen bond

Hydrogen bonding significantly influenced the strength and specificity of the protein-ligand interactions. Recognizing the crucial role of hydrogen bonds in complex stability, their formation between c-Myc and the promising ligands was monitored throughout the 100 ns MD simulations to assess the dynamic stability of the complexes. As shown in Figure 6, the results revealed varying levels of hydrogen bond formation across the complexes. The c-Myc_Alisertib and c-Myc_Broussoflavonol F complexes exhibited the most robust hydrogen bonding network, with four bonds observed in each. The c-Myc_Ellagic acid complex formed three hydrogen bonds, while the c-Myc_Artonin M and c-Myc_Cycloaltilisin 7 complexes each formed two hydrogen bonds. These findings suggest that Alisertib and Broussoflavonol F may establish more stable complexes with c-Myc, potentially resulting in stronger binding interactions. Furthermore, Figure 7 depicts the distribution of hydrogen bonds (within 0.3 nm) within the protein-ligand complexes, providing insights into the interactions of compounds exhibiting stronger binding affinities than Alisertib.

3.3.4. Radius of gyration (ROG)

The Radius of Gyration (Rg) was evaluated and visualized in Figure 8 to ascertain the compactness variations of the protein-ligand complexes. The control drug, Alisertib, exhibited high Rg fluctuations compared to other compounds, indicating greater variations in the overall shape of the complex. Ellagic acid experienced fluctuations until approximately 50 ns, after which it regained stability. Notably, Artonin M and Broussoflavonol F maintained relatively constant Rg values throughout the entire simulation, suggesting consistent compactness of these complexes. Cycloaltilisin 7 showed a deviation between 78 ns and 89 ns before regaining stability. These Rg results corroborate the RMSD findings, particularly highlighting the stability of the Artonin M and Broussoflavonol F complexes.

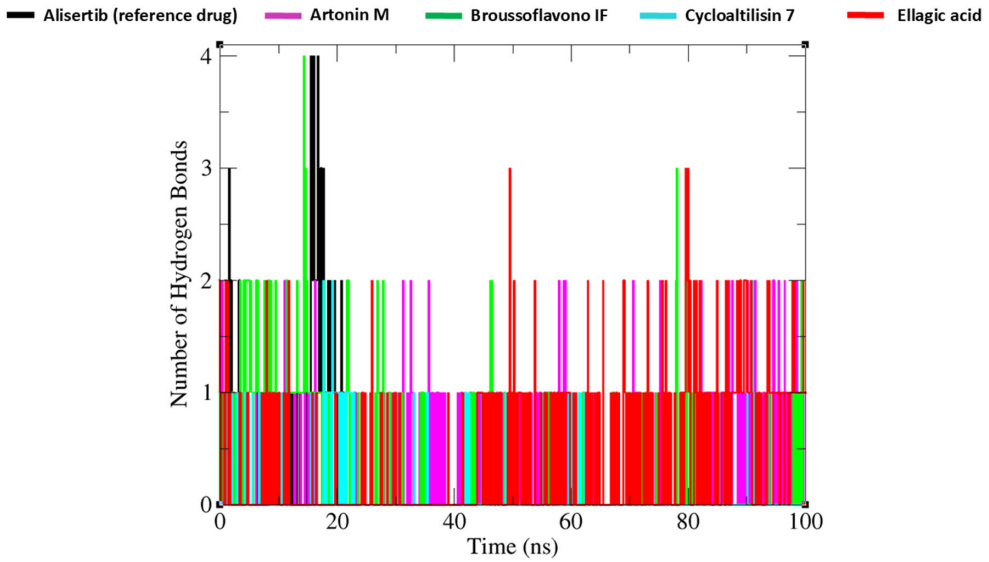

Figure 6. Graph depicting the number of intermolecular H-bonds formed between protein-ligand complexes of selected ligands and the reference drug (Alisertib)

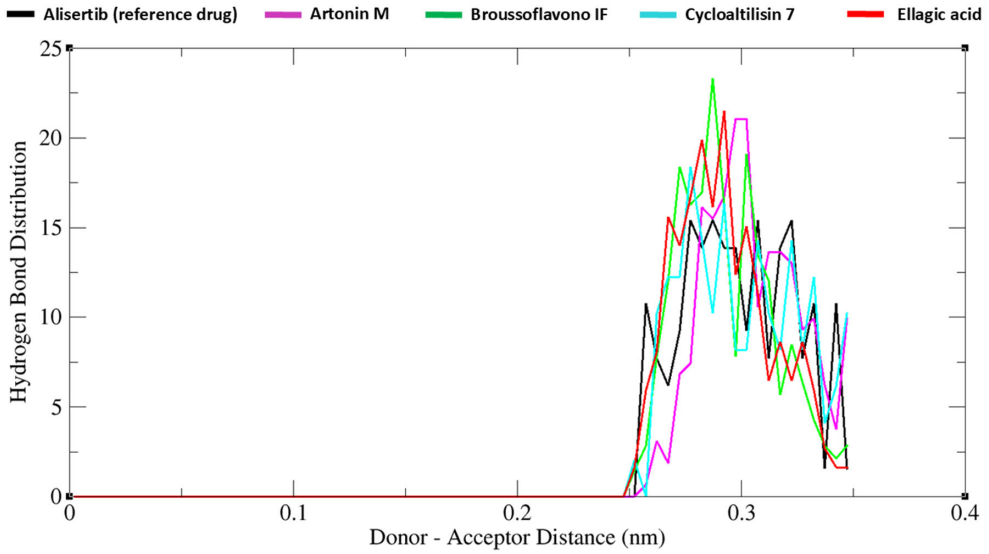

Figure 7. H-bond distribution (within 0.3 nm distance) for protein-ligand complex of the selected ligands in comparison to the reference drug (black)

3.3.5. SASA

The SASA of the complexes was evaluated during the simulation, as shown in Figure 9. This analysis offers valuable insights into the extent of the complexes' exposure to the surrounding solvent environment. The c-Myc_Alisertib complex initially exhibited a SASA of 91.5 nm^2, which decreased to 83 nm^2 as the simulation progressed, indicating a reduction in solvent exposure. The other complexes showed varying degrees of solvent accessibility: c-Myc_Ellagic_acid (92.8 nm^2), c-Myc_ArtoninM (89.25 nm^2), c-Myc_Cycloaltilisin 7 (90.5 nm^2), and c-Myc_BroussoflavonolF (92 nm^2). The lower SASA value for the Artonin M complex suggests a more compact structure with less solvent exposure, which aligns with its stability observed in the RMSD and Rg analyses.

3.4. Molecular Mechanics Poisson-Boltzmann Surface Area (MM-PBSA)

The MM-PBSA calculations provided quantitative support for the superior ligand-protein interaction strength of these compounds. Broussoflavonol F exhibited the most favorable interaction with a calculated energy of −23.84 kcal/mol, followed closely by Artonin M at −17.88 kcal/mol. Ellagic acid (−10.57 kcal/mol) and Cycloaltilisin 7 (−8.80 kcal/mol) also demonstrated stronger interactions compared to Alisertib (−2.70 kcal/mol), as detailed in Table 4. The energy component analysis revealed that Broussoflavonol F and Artonin M benefit from strong van der Waals interactions and a favorable balance between electrostatic and solvation effects, explaining their superior performance across different analyses.

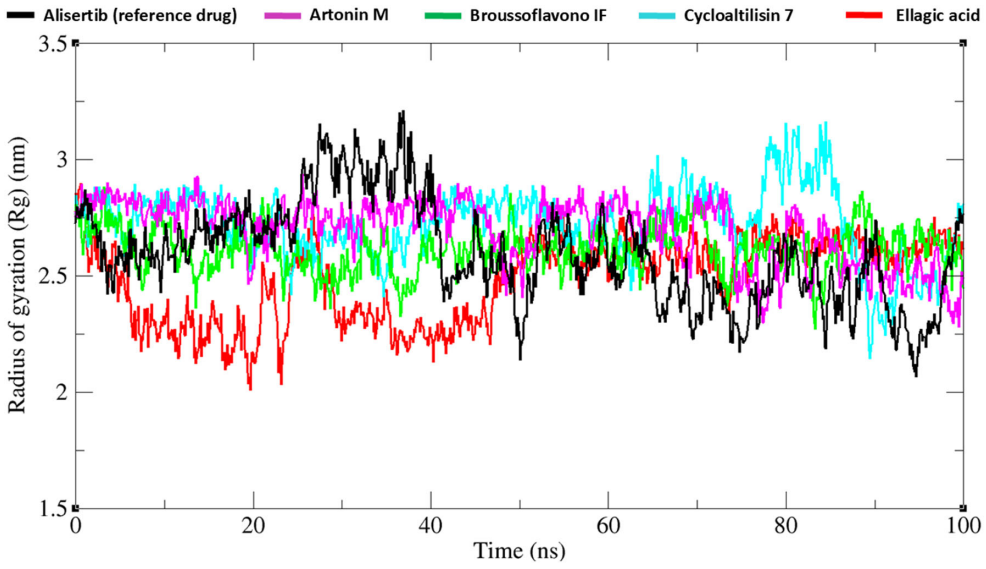

Figure 8. Radius of gyration plot

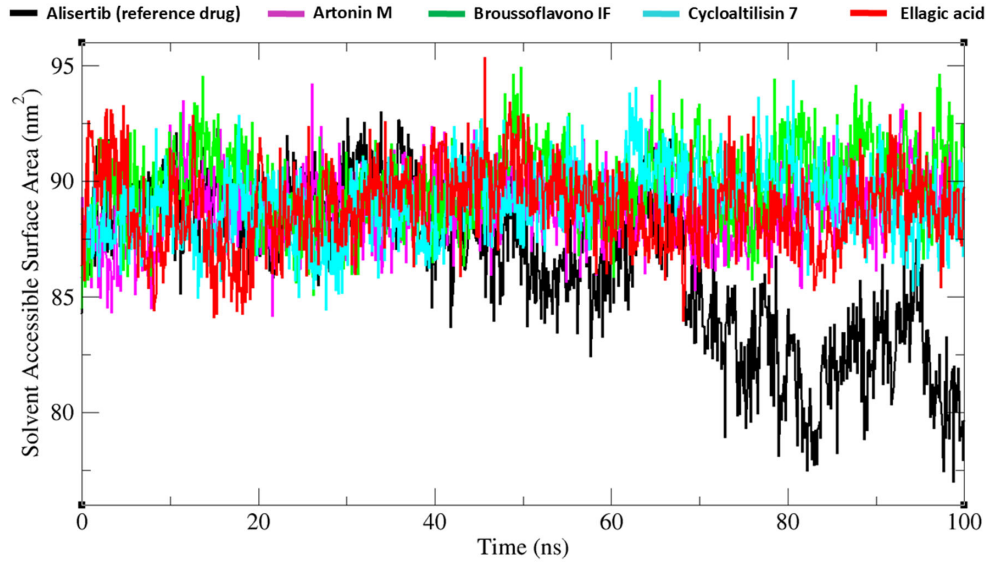

Figure 9. Solvent-accessible surface area plot

Table 4. MM-PBSA binding energy calculations for top-ranked ligands

S. No.	Compound ID	$\Delta G_{VDWaals}$ (kcal/mol)	ΔG_{EEL} (kcal/mol)	ΔG_{EPB} (kcal/mol)	$\Delta G_{ENPolar}$ (kcal/mol)	ΔG_{gas} (kcal/mol)	ΔG_{solv} (kcal/mol)	ΔG_{total} (kcal/mol)
1.	Alisertib (reference)	−3.57	−40.79	42.17	−0.51	−44.36	41.66	−2.70
2.	Artonin M	−33.76	−18.16	37.62	−3.58	−51.92	34.04	−17.88
3.	Broussoflavonol F	−36.48	−10.50	27.07	−3.93	−46.97	23.14	−23.84
4.	Cycloaltilisin7	−15.51	−2.10	10.67	−1.86	−17.61	8.81	−8.80
5.	Ellagic acid	−19.84	−6.11	17.68	−2.30	−25.95	15.38	−10.57

The molecular dynamics simulations provided valuable insights into the stability and dynamic behavior of the protein-ligand complexes. The exceptional stability of Broussoflavonol F, as evidenced by its low RMSD and favorable Rg values, aligns with previous studies emphasizing the importance of dynamic stability in drug design [29]. However, the unexpected fluctuations observed in the Cycloaltilisin 7 complex suggest that further investigation is needed to understand its binding mechanism.

Future studies should progress from computational predictions to experimental validation, beginning with in vitro evaluation of candidate compounds (ellagic acid, artonin M, cycloaltilisin 7, and Broussoflavonol F) in c-MYC-driven cancer models, followed by in vivo assessment using xenograft systems. Our findings both confirm and extend previous work on c-MYC inhibition – while prior studies focused on synthetic bHLH domain-targeting molecules, we demonstrate comparable efficacy from natural *Artocarpus altilis*-derived compounds. The promising computational results for these candidates, particularly their binding affinities and pharmacokinetic profiles, warrant rigorous preclinical validation before clinical development.

4. Conclusion

This study employed a comprehensive in silico approach to identify and evaluate *Artocarpus altilis*-derived compounds as potential c-MYC inhibitors. Through molecular docking, pharmacokinetic analysis, and molecular dynamics simulations, four compounds – Broussoflavonol F, Artonin M, Ellagic acid, and Cycloaltilisin 7 – demonstrated superior binding affinities and stability compared to the reference drug Alisertib. Notably, Broussoflavonol F exhibited the most favorable MM-PBSA binding energy (−23.84 kcal/mol) and exceptional stability during molecular dynamics simulations, making it a strong candidate for further development as a lead compound. These findings align with previous studies on natural compounds as c-MYC inhibitors but also highlight the unique potential of *Artocarpus altilis*-derived compounds. However, the potential toxicity concerns, particularly for Artonin M and Ellagic acid, underscore the need for further optimization. Future research should focus on experimental validation and structural modifications to improve the pharmacokinetic profiles of these compounds, offering a promising strategy for targeting c-MYC-driven cancers.

Conflicts of Interest

The authors declare that they have no conflicts of interest to this work.

Data Availability Statement

The data that support this work are available upon reasonable request to the corresponding author.

Author Contribution Statement

Tomilola Victor Akingbade: Methodology, Software, Validation, Formal analysis, Investigation, Resources, Data curation, Writing – original draft, Writing – review & editing, Visualization, Supervision, Project administration. **Ayobami Fidelix:** Conceptualization, Methodology, Software, Validation, Formal analysis, Investigation, Resources, Writing – original draft, Writing – review & editing, Supervision, Project administration. **Jatin Jangra:** Software, Investigation, Visualization. **Olutola Adeyemo:** Data curation, Writing – original draft, Writing – review & editing. **Damilola Adeniyi:** Validation, Data curation, Writing – original draft, Writing – review & editing. **Dolapo Damilola Akinlose:** Formal analysis, Resources, Writing – original draft, Writing – review & editing.

References

[1] Jha, R. K., Kouzine, F., & Levens, D. (2023). MYC function and regulation in physiological perspective. *Frontiers in Cell and Developmental Biology*, *11*, 1268275. https://doi.org/10.3389/fcell.2023.1268275

[2] Duffy, M. J., O'Grady, S., Tang, M., & Crown, J. (2021). MYC as a target for cancer treatment. *Cancer Treatment Reviews*, *94*, 102154. https://doi.org/10.1016/j.ctrv.2021.102154

[3] Dhanasekaran, R., Deutzmann, A., Mahauad-Fernandez, W. D., Hansen, A. S., Gouw, A. M., & Felsher, D. W. (2022). The *MYC* oncogene—The grand orchestrator of cancer growth and immune evasion. *Nature Reviews Clinical Oncology*, *19*(1), 23–36. https://doi.org/10.1038/s41571-021-00549-2

[4] Llombart, V., & Mansour, M. R. (2022). Therapeutic targeting of "undruggable" MYC. *eBioMedicine*, *75*, 103756. https://doi.org/10.1016/j.ebiom.2021.103756

[5] Madden, S. K., Dantas de Araujo, A., Gerhardt, M., Fairlie, D. P., & Mason, J. M. (2021). Taking the Myc out of cancer: Toward therapeutic strategies to directly inhibit c-Myc. *Molecular Cancer*, *20*(1), 3. https://doi.org/10.1186/s12943-020-01291-6

[6] Scafuro, M., Capasso, L., Carafa, V., Altucci, L., & Nebbioso, A. (2021). Gene transactivation and transrepression in MYC-driven cancers. *International Journal of Molecular Sciences*, *22*(7), 3458. https://doi.org/10.3390/ijms22073458

[7] Rahl, P. B., & Young, R. A. (2014). MYC and transcription elongation. *Cold Spring Harbor Perspectives in Medicine*, *4*(1), a020990. https://doi.org/10.1101/cshperspect.a020990

[8] Balaratnam, S., & Schneekloth, J. S. (2020). Transcriptional regulation of MYC through G-quadruplex structures. *Annual Reports in Medicinal Chemistry*, *54*, 361–407. https://doi.org/10.1016/bs.armc.2020.05.002

[9] Chen, G. S., Chen, S. Y., Liu, S. T., Hsieh, C. C., Lee, S. P., & Huang, S. M. (2022). Stabilization of the c-Myc protein via the modulation of threonine 58 and serine 62 phosphorylation by the disulfiram/copper complex in oral cancer cells. *International Journal of Molecular Sciences*, *23*(16), 9137. https://doi.org/10.3390/ijms23169137

[10] Kotekar, A., Kumar Singh, A., & Devaiah, B. N. (2023). BRD4 and MYC: Power couple in transcription and disease. *The FEBS Journal*, *290*(20), 4820–4842. https://doi.org/10.1111/febs.16580

[11] Shah, K., Ansari, M., Saeed, S., Wali, A., & Mushtaq Yasinzai, M. (2024). Nilotinib: Disrupting the MYC-MAX heterocomplex. *Bioinformatics and Biology Insights*, *18*, 11779322241267056. https://doi.org/10.1177/11779322241267056

[12] Singh, A., Kumar, A., Kumar, P., Nayak, N., Bhardwaj, T., Giri, R., & Garg, N. (2021). A novel inhibitor L755507 efficiently blocks c-Myc–MAX heterodimerization and induces apoptosis in cancer cells. *Journal of Biological Chemistry*, *297*(1), 100903. https://doi.org/10.1016/j.jbc.2021.100903

[13] Atanasov, A. G., Zotchev, S. B., Dirsch, V. M., & Supuran, C. T. (2021). Natural products in drug discovery: Advances and opportunities. *Nature Reviews Drug Discovery*, *20*(3), 200–216. https://doi.org/10.1038/s41573-020-00114-z

[14] Buddhisuharto, A. K., Pramastya, H., Insanu, M., & Fidrianny, I. (2021). An updated review of phytochemical compounds and pharmacology activities of Artocarpus genus. *Biointerface Research in Applied Chemistry*, *11*(6), 14898–14905. https://doi.org/10.33263/BRIAC116.1489814905

[15] Soifoini, T., Donno, D., Jeannoda, V., Rakoto, D. D., Msahazi, A., Farhat, S. M. M., . . . , & Beccaro, G. L. (2021). Phytochemical composition, antibacterial activity, and antioxidant properties of the *artocarpus altilis* fruits to promote their consumption in the Comoros islands as potential health-promoting food or a source of bioactive molecules for the food industry. *Foods*, *10*(9), 2136. https://doi.org/10.3390/foods10092136

[16] Sammak, S., Hamdani, N., Gorrec, F., Allen, M. D., Freund, S. M. V., Bycroft, M., & Zinzalla, G. (2019). Crystal structures and nuclear magnetic resonance studies of the apo form of the c-MYC: MAX bHLHZip complex reveal a helical basic region in the absence of DNA. *Biochemistry*, *58*(29), 3144–3154. https://doi.org/10.1021/acs.biochem.9b00296

[17] Fidelix, A., Akingbade, T., Jangra, J., Olabuntu, B., Adeyemo, O., & Akingbade, J. (2025). In Silico study and validation of natural compounds derived from *Macleaya cordata* as a potent inhibitor for BTK. *Medinformatics*, *2*(1), 22–35. https://doi.org/10.47852/bonviewMEDIN52024239

[18] Schrödinger (2025). *PyMOL* [Computer software]. http://www.pymol.org/pymol

[19] Wallace, A. C., Laskowski, R. A., & Thornton, J. M. (1995). LIGPLOT: A program to generate schematic diagrams of protein-ligand interactions. *Protein Engineering, Design & Selection*, *8*(2), 127–134. https://doi.org/10.1093/protein/8.2.127

[20] Daina, A., Michielin, O., & Zoete, V. (2017). SwissADME: A free web tool to evaluate pharmacokinetics, drug-likeness and medicinal chemistry friendliness of small molecules. *Scientific Reports*, *7*(1), 42717. https://doi.org/10.1038/srep42717

[21] Pires, D. E. V., Blundell, T. L., & Ascher, D. B. (2015). pkCSM: Predicting small-molecule pharmacokinetic and toxicity properties using graph-based signatures. *Journal of Medicinal Chemistry*, *58*(9), 4066–4072. https://doi.org/10.1021/acs.jmedchem.5b00104

[22] Abraham, M. J., Murtola, T., Schulz, R., Páll, S., Smith, J. C., Hess, B., & Lindahl, E. (2015). GROMACS: High performance molecular simulations through multi-level parallelism from laptops to supercomputers. *SoftwareX*, *1–2*, 19–25. https://doi.org/10.1016/j.softx.2015.06.001

[23] Jo, S., Kim, T., Iyer, V. G., & Im, W. (2008). CHARMM-GUI: A web-based graphical user interface for CHARMM. *Journal of Computational Chemistry*, *29*(11), 1859–1865. https://doi.org/10.1002/jcc.20945

[24] Humphrey, W., Dalke, A., & Schulten, K. (1996). VMD: Visual molecular dynamics. *Journal of Molecular Graphics*, *14*(1), 33–38. https://doi.org/10.1016/0263-7855(96)00018-5

[25] Winter, A. (2022). *QtGrace: Native Grace for Windows, Linux and Mac OS X based on Qt* (Beta) [Computer software]. SourceForge. https://sourceforge.net/projects/qtgrace/

[26] Wang, E., Sun, H., Wang, J., Wang, Z., Liu, H., Zhang, J. Z. H., & Hou, T. (2019). End-point binding free energy calculation with MM/PBSA and MM/GBSA: Strategies and applications in drug design. *Chemical Reviews*, *119*(16), 9478–9508. https://doi.org/10.1021/acs.chemrev.9b00055

[27] Valdés-Tresanco, M. S., Valdés-Tresanco, M. E., Valiente, P. A., & Moreno, E. (2021). gmx_MMPBSA: A new tool to perform end-state free energy calculations with GROMACS. *Journal of Chemical Theory and Computation*, *17*(10), 6281–6291. https://doi.org/10.1021/acs.jctc.1c00645

[28] Cierpicki, T., & Grembecka, J. (2015). Targeting protein–protein interactions in hematologic malignancies: Still a challenge or a great opportunity for future therapies? *Immunological Reviews*, *263*(1), 279–301. https://doi.org/10.1111/imr.12244

[29] Shin, W. H., Kumazawa, K., Imai, K., Hirokawa, T., & Kihara, D. (2020). Current challenges and opportunities in designing protein–protein interaction targeted drugs. *Advances and Applications in Bioinformatics and Chemistry*, *13*, 11–25. https://doi.org/10.2147/AABC.S235542

[30] Lu, H., Zhou, Q., He, J., Jiang, Z., Peng, C., Tong, R., & Shi, J. (2020). Recent advances in the development of protein–protein interactions modulators: Mechanisms and clinical trials. *Signal Transduction and Targeted Therapy*, *5*(1), 213. https://doi.org/10.1038/s41392-020-00315-3

[31] Juvale, I. I. A., Abdul Hamid, A. A., Abd Halim, K. B., & Che Has, A. T. (2022). P-glycoprotein: New insights into structure, physiological function, regulation and alterations in disease. *Heliyon*, *8*(6), e09777. https://doi.org/10.1016/j.heliyon.2022.e09777

[32] Zhao, M., Ma, J., Li, M., Zhang, Y., Jiang, B., Zhao, X., . . . , & Qin, S. (2021). Cytochrome P450 enzymes and drug metabolism in humans. *International Journal of Molecular Sciences*, *22*(23), 12808. https://doi.org/10.3390/ijms222312808

[33] Garrido, A., Lepailleur, A., Mignani, S. M., Dallemagne, P., & Rochais, C. (2020). hERG toxicity assessment: Useful guidelines for drug design. *European Journal of Medicinal Chemistry*, *195*, 112290. https://doi.org/10.1016/j.ejmech.2020.112290

How to Cite: Akingbade, T. V., Fidelix, A., Jangra, J., Adeyemo, O., Adeniyi, D., & Akinlose, D. D. (2025). In Silico Design of Novel *Artocarpus altilis*-Derived Compounds Targeting the c-Myc/Max Heterodimer. *Medinformatics*, *2*(3), 181–194. https://doi.org/10.47852/bonviewMEDIN52024995

Supplementary Information

(A)	(B)
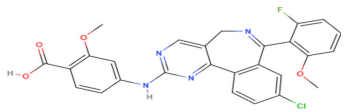	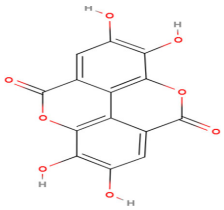
(C)	(D)
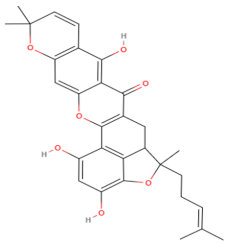	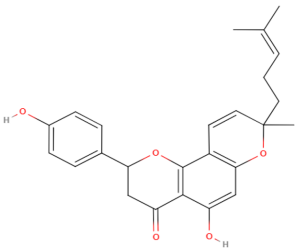
(E)	(F)
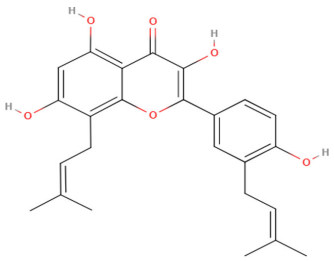	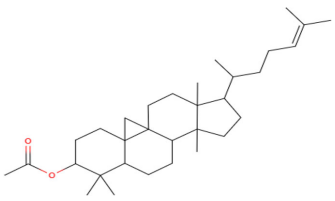
(G)	(H)
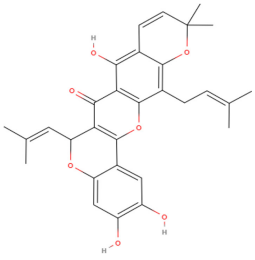	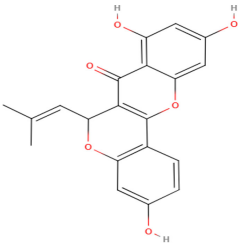

(I)	(J)
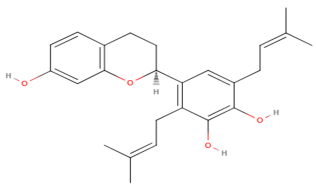	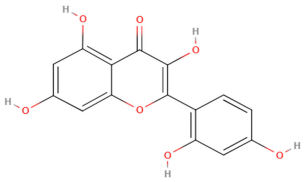
(K)	
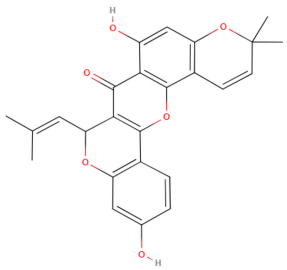	

Supplementary Figure 1. Structures of bioactive compounds discussed in the manuscript. (A) Alisertib. (B) Ellagic acid. (C) Artonin M. (D) Cycloaltilisin 7. (E) Broussoflavonol F. (F) Cycloartenyl acetate. (G) Cycloheterophyllin. (H) Cyclocommunol. (I) Kazinol A. (J) Morin. (K) Cyclomorusin.